2015 IEEE 28th International Symposium on Computer-Based Medical Systems

Stitched Multipanel Biomedical Figure Separation

K.C. Santosh, Sameer Antani, George Thoma
National Library of Medicine, National Institutes of Health
8600 Rockville Pike, Bethesda, MD 20894, USA
Email: {santosh.kc, sameer.antani, george.thoma}@nih.gov

***Abstract*—We present a novel technique to separate subpanels from stitched multipanel figures appearing in biomedical research articles. Since such figures may comprise images from different imaging modalities, separating them is a critical first step for effective biomedical content-based image retrieval (CBIR). The method applies local line segment detection based on the gray-level pixel changes. It then applies a line vectorization process that connects prominent broken lines along the subpanel boundaries while eliminating insignificant line segments within the subpanels. We have validated our fully automatic technique on a subset of stitched multipanel biomedical figures extracted from articles within the Open Access subset of PubMed Central repository, and have achieved precision and recall of 81.22% and 85.08%, respectively.**

***Index Terms*—Automation; line segment detection; stitched multipanel figures; biomedical publications; content-based image retrieval.**

I. Introduction

A. Motivation

Figures in the scientific publications provide a unique source of information that typically complements the facts described in the text. In biomedical image retrieval [1]–[5], figures are often composed of multiple panels, each describing different methodologies, modalities or results, including the possibility of providing direct comparisons among them. In this domain, authors report an increasing use of medical images [6], [7]. The average number of figures in reputable biomedical journals ranges from 6 to 31 [8], [9]. More importantly, according to [10]–[12], multipanel figures represent about 50% of the figures in the biomedical open access articles used for the imageCLEF (URL: http://www.imageclef.org) benchmark. However, such figures pose a challenge for image retrieval [1]–[3], [13] and modality classification systems [5], [14], [15]. We also note that these figures are not commonly available in biomedical datasets as standalone entities that could be readily used by automated systems since only a few databases require authors to submit figures (and captions) in separate files for easy access. In other words, most of the figures are embedded in the article, thereby reducing their automatic accessibility [16]. In this context, multipanel figure separation is considered as a crucial step, assuming that each subpanel contains a single modality. By doing so, it improves the performance of CBIR [4], [16]–[18], and hence is a precursor to biomedical CBIR.

B. Related work

Multipanel figure separation does not have rich state-of-the-art approaches. Projection profile-based methods are commonly used (and fairly sufficient) to separate subpanels of those figures, which are having homogeneous gaps between them [17], [19]. Either of the two penetrations (using horizontal and vertical profiles) helps to separate them (i.e., two different levels of separations are required [17], [18]). But, when homogeneous gaps do not penetrate from left to right and top to bottom, straightforward projection profiles fail to separate subpanels. As a consequence, it requires integration of heuristics, which may not be generalized. In Fig. 1, no homogeneous gaps are provided between the subpanels and therefore, this problem is beyond their scope. Other approaches integrate subpanel labels with image-based separation via the use of bounding boxes of connected components [16], [18]. In [16], experimental results show that their solution is sensitive to common errors generated by the optical character recognition (OCR). Texts that are overlaid in complex background having large contrast variations cause significant OCR performance reduction. Further, layout graphs are used to detect missed nodes (i.e., panel labels). The proposed graph may not be accurate in case subpanel labels are not appeared in a regular fashion (i.e., equal number of columns in all rows, like tabular format). Figs. 1 (f) and (g) are two examples of it. Another difficulty will be high number of content bearing texts (within the subpanels that effectively summarize the facts) can make confusions with panel labels [16]. These problems remain the same for recently reported work [18]. They, however, integrate several heuristics to solve specific problems. For example, thresholds ranging from 50 to 200 (by calling them as empirically designed intensity values) do not apply in general, for binarization. Such a binarization may not work in case figures having different colors associated with different subpanels (see Figs. 1) (e), (f), (g) and (j)). In [18], authors claim the usefulness of panel labels (by projecting text labels orthogonally) in detecting sub-panels. On the other hand, they do not argue about the possible absence as well as irregularities of text labels on the whole (see Figs. 1 (f), (g) and (j)). Moreover, figures having rectangular boxes (with no panel labels) appeared in a zig-zag fashion are beyond the scope of the state-of-the-art, in general.

Overall, in the literature, uniform-space-separated multipanel figures comprise a significant portion of the dataset used to evaluate their systems, including graphical illustrations,

2372-9198 2015

DOI 10.1109/CBMS.2015.51

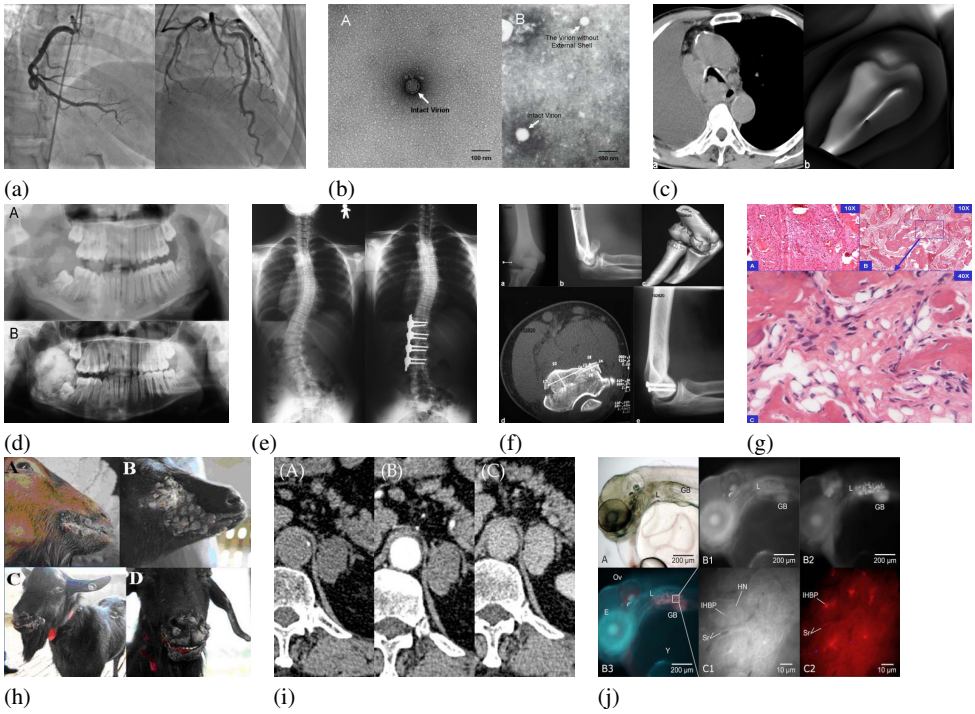

Fig. 1. Examples showing stitched multipanel figures. These are appeared with and without panel labels, including irregular panel boxes.

plots/curves. Other methods address panel label integration by using OCR for fully connected multipanel figures, which we call 'stitched' multipanel figures. But, none of the methods were focused to separate fully connected multipanel figures from an image analysis standpoint. One of the primary reasons that has been commonly stated is, no clear boundaries and no homogeneous gaps exist between the subpanels. In this paper, we address the challenging task of separating such stitched subpanels (as depicted in Fig. 1).

II. Materials & Methods

A. Outline

As shown in Fig. 2, considering the nature of the problem, our method aims to detect subpanel boundaries. Starting from an edge enhanced image as shown in Fig. 2 (a), we detect line segments along the edges (see Fig. 2 (b)). These line segments are filtered using line filters defined in two orthogonal directions: 0 and $\pi/2$, which is followed line vectorization process. Profile-based line vectorization connects broken line segments and provides end-to-end penetrations as shown Fig. 2 (c). Subpanels are then separated/cropped from a complete figure by using four corners at line crossings (see Fig. 2 (d - e)), representing rectangles.

B. Line segment detector

Before detecting straight contours (i.e., line segments), we perform edge enhancement. It identifies sharp edge boundaries, such as the edge between a subject and a background of a contrasting color, and increases the image contrast in the area immediately around the edge. For this, we use standard deviation of the Gaussian low pass filter in addition to the use of strength of the sharpening effect and minimum contrast threshold (between 0 and 1) required for a pixel to be considered as an edge pixel.

Line segment detector (LSD) aims to detect local straight contours (i.e., line segments), from the zones where the gray-level pixel changes from dark to light or vice-versa [20]. It uses two concepts: the gradient and the level-lines. The image gradient is computed at each pixel using a 2×2 mask (which is the smallest possible mask size), $\begin{bmatrix} \mathbf{f}(x,y) & \mathbf{f}(x+1,y) \\ \mathbf{f}(x,y+1) & \mathbf{f}(x+1,y+1) \end{bmatrix}$, where $\mathbf{f}(x,y)$ is the gray-level value at pixel (x,y). The image gradient ($g_x(x,y)$ and $g_y(x,y)$) and the level-line direction (θ) can be computed as follows:

$$g_x = \left(\mathbf{f}(x+1,y) + \mathbf{f}(x+1,y+1) - \mathbf{f}(x,y) - \mathbf{f}(x,y+1)\right)/2,$$
$$\theta = \arctan\left(g_x/g_y\right), \quad (1)$$

where g_y is computed as g_x, and the gradient magnitude is, $G(x,y) = \left(g_x(x,y) + g_y(x,y)\right)^{1/2}$. The gradient and level-line angles encode the direction of the edge. For more detailed information about implementation, we refer to [20]. In Fig. 3, line segment detection is shown along the subpanel boundary.

C. Subpanel boundary detection via line segments

An advantage of such a generic LSD tool is that it can extract a set of lines, $\mathcal{L}$, having different lengths in all possible orientations, $\mathcal{L} = \{\ell_{i,\theta}\}_{i=1,\ldots,\mathbf{L}}$ and $\theta \in [0, 2\pi)$. Such a complete set $\mathcal{L}$ is composed of line segments not only from subpanel boundaries but also from the objects within subpanels.To preserve the line segments representing subpanel boundaries, we perform the following two consecutive processes:

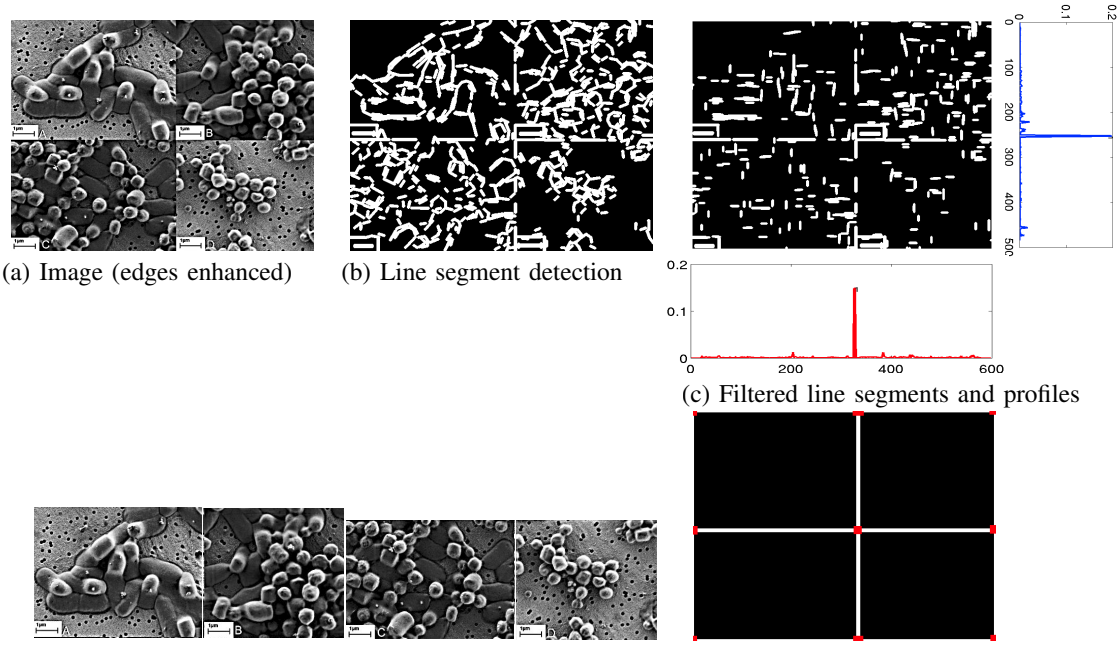

(a) Image (edges enhanced) (b) Line segment detection (c) Filtered line segments and profiles

(e) Output: subpanels (s_1 to s_4) separation (d) Line vectorization and corner detection (in red)

Fig. 2. A complete workflow of the proposed algorithm: (a) studied image with edges enhanced, (b) line segment detection that follows the gray-level pixel changes between neighboring pixels, (c) projection profiles of the filtered line segments using line filters defined in two orthogonal directions: 0 and $\frac{\pi}{2}$, (d) Profile-based line vectorization and corner detection at line crossings (e) subpanel figures (s_1 to s_4) separation using rectangles that are composed of four corners.

1) convolution of all line segments ($\ell \in \mathcal{L}$) with the predefined set $\mathcal{K}$ of kernels, representing the line segments of subpanel boundaries; and
2) profile-based line vectorization to connect prominent broken lines belonging to the subpanel boundaries while eliminating unnecessary line segments within the subpanels.

Convolution. For this, we construct a set $\mathcal{K}$ of kernels,

$$\mathcal{K} = \{k_j\}_{j=1,\ldots,\mathbf{K}}, \text{ and } k = \mathbf{f}('line', len, \theta) \quad (2)$$

where any jth k represents a linear structuring element. In general, we define a binary kernel representing a line of any particular length len and angle θ, $k = \mathbf{f}('line', len, \theta)$. In a discrete case, a structuring element can be represented as a set of pixels on a grid, assuming the value 1 if the pixel belongs to the structuring element or 0, otherwise [21]. As an example, kernel k of $len = 5$ at different angles $\theta = 0$ and $\pi/6$ can respectively, be represented by

$$\begin{bmatrix}1 & 1 & 1 & 1 & 1\end{bmatrix} \text{ and } \begin{bmatrix}0 & 0 & 0 & 1 & 1\\ 0 & 0 & 1 & 0 & 0\\ 1 & 1 & 0 & 0 & 0\end{bmatrix}.$$

Orientation of biomedical figures is assumed to up upright (i.e., they are not rotated). We are required to filter line segments in two orthogonal directions: 0 and $\pi/2$, and therefore, we have $\mathcal{K} = \{k_1, k_2\}$. Using these two kernels (of length 10 pixels, empirically designed), we perform convolution with all possible line segments, $\mathcal{L}' = \mathcal{L} \otimes \mathcal{K}$, where $\mathcal{L}' \in \mathcal{L}$. The set $\mathcal{L}'$ represents all line segments in two orthogonal directions (i.e., 0 and $\pi/2$). Fig. 2 (c) shows an example, where most of the line segments that are appeared within the subpanels are eliminated.

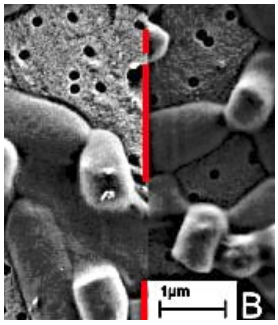

(zoomed: $\times 1.4$)

Fig. 3. An example showing line segment detection along the subpanel boundary. Line segments along the subpanel boundaries do not pass end to end. For this illustration, a small portion of the image is cropped from Fig. 2.

Profile-based line vectorization. Keeping spatial information of the line segments $\ell'_i \in \mathcal{L}'$, we compute orthogonal projection profiles in both directions: 0 and $\pi/2$. These profiles are used to separate multipanel figures from where the most prominent peaks are detected. Assuming that the prominent peaks are mostly seen along the subpanel boundaries, they are useful to process line vectorization. This process connects

broken line segments (see Fig. 3, as an example) along the subpanel boundaries.

Projection profiles from a 2D image $\mathbf{f}(x, y)$ of size $m \times n$ can be computed as

$$p_{\theta=\pi/2} = \sum_{1 \le x \le m} \mathbf{f}(x, y) \text{ and } p_{\theta=0} = \sum_{1 \le y \le n} \mathbf{f}(x, y). \quad (3)$$

To eliminate dominant line segments that typically result from objects within the subpanels, we compute their corresponding profile transforms (i.e., p^2_θ), which is then normalized by using their mean and standard deviation. As a consequence, the magnitude of the line segments along subpanel boundaries are more pronounced and detected accordingly. Fig. 2 (c) shows an example. Peak(s) is(are) detected based on the empirically designed threshold that uses the studied image size (i.e., height h and width w): $\wp_h, \wp_v \ge 0.4 \times h, w$, where $\wp$ is the detected peak from a profile p. From the location where peak(s) are detected, line(s) is(are) extended from end to end (in both directions).

In this process, we assume normalized peak heights are closer $\hat{\wp}_h \simeq \hat{\wp}_v$ (like in Fig. 2 (c)). In case $\hat{\wp}_h \ll \hat{\wp}_v$, row-wise line vectorization (i.e., horizontal subpanel separation) is done first, which is followed by column-wise line vectorization or vice versa.

D. Subpanel separation via corners at line crossings

To detect line crossings, we use Harris corner detector [22], since it considers the differential of the corner score with respect to line (edge) direction. The algorithm depends on the eigenvalues of the summation of the squared difference matrix (SSD). The eigenvalues of an SSD matrix represent the differences between the surroundings of a pixel and the surroundings of its neighbors. The larger the difference between the surroundings of a pixel and those of its neighbors, the larger the eigenvalues. The larger the eigenvalues, the more likely that a pixel appears at a corner. Fig. 2 (d) shows an example, where corners (in red) are highlighted.

Subpanels are separated based on the set $\mathcal{C}$ of detected corners, $\mathcal{C} = \{c_i\}_{i=1,\ldots,\mathbf{C}}$, where $c = (x, y)$. Starting from the leftmost corner, any subpanel can be separated by selecting four coordinate points so that it can be transformed into a rectangle, $r_i = [c_i, r_{width}, r_{height}]$, where c_i is the coordinate point from which any ith rectangle r is drawn. This allows subpanel cropping easier.

To eliminate empty rectangles (see Fig. 4), the algorithm checks image information about pixel information within the subpanel (i.e., by computing an image histogram). In Fig. 4, empty rectangles are pruned since such cropped images (considered as subpanels) with no information will not be useful for image retrieval or classification problem.

III. Experiments

A. Dataset and ground-truth formation

Even though the goal remains the same, evaluations of the state-of-the-art methods vary with the dataset collection. But, most of the reported methods used imageCLEF. However, none of them evaluated stitched multipanel figures.

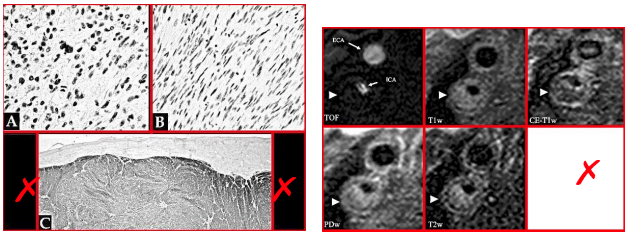

(a) (b)

Fig. 4. Examples showing empty rectangle elimination. Subpanels that are checked with cross mark (in red) are eliminated.

Besides the imageCLEF, we used NLM's *Open-i* (URL: http://openi.nlm.nih.gov) search engine to collect more samples, where subpanels are completely connected. Altogether, our collection is composed of 150 images, and are available upon request. A few samples are shown in Fig. 1. For validation purpose, we developed an annotator that can automatically annotate the subpanels in the presence of the user.

B. Evaluation protocol

For any image I, we have a set $\mathcal{R}$ of the detected rectangles: $I \mapsto \mathcal{R}$ and $\mathcal{R} = \{r_i\}_{i=1,\ldots,\mathbf{R}}$, representing an output. Similarly, the annotator produces a set $\mathcal{R}^\circ$ of ground-truths, $\mathcal{R}^\circ = \{r^\circ_i\}_{i^\circ=1,\ldots,\mathbf{R}^\circ}$. Each rectangle refers to a subpanel.

For validation, for any given image in the dataset, our performance evaluation criteria are precision, recall and F_1-score. In general, these metrics can be expressed as follows:

$$\text{precision} = \frac{\mathbf{c}}{\mathbf{R}},$$
$$\text{recall} = \frac{\mathbf{c}}{\mathbf{R}^\circ} \text{ and}$$
$$\mathrm{F}_1\text{-score} = 2\left(\frac{(\mathbf{c}/\mathbf{R}) \times (\mathbf{c}/\mathbf{R}^\circ)}{(\mathbf{c}/\mathbf{R}) + \mathbf{c}/\mathbf{R}^\circ)}\right), \quad (4)$$

where c is the number of correct matches from the detected set $\mathbf{R}$ and $\mathbf{R}^\circ$ is the total number of rectangles (in the ground-truth) that are expected to be detected. The score computed from every metric is normalized by total number of images in the database.

To compute the aforementioned metrics, overlapping ratio (OR) is used to identify the number of correct matches $\mathbf{c}$. Consider two rectangles: r° and r, their OR can be computed as [23]

$$\text{OR}(r^\circ, r) = \frac{2 \times |r^\circ \cap r|}{|r^\circ| + |r|} \text{ and } \text{OR}(,) \in [0, 1], \quad (5)$$

where $|r^\circ \cap r|$ is the intersected or common area, and $|r^\circ|$ and $|r|$ are the individual areas. When separating subpanels, we may not achieve 100% OR since a few border pixels can possibly be chopped. Therefore, we follow the following condition:

$$\mathbf{c} = \begin{cases} 1 : \text{if OR}(,) \ge 0.8 \text{ and} \\ 0 : \text{ otherwise.} \end{cases} \quad (6)$$

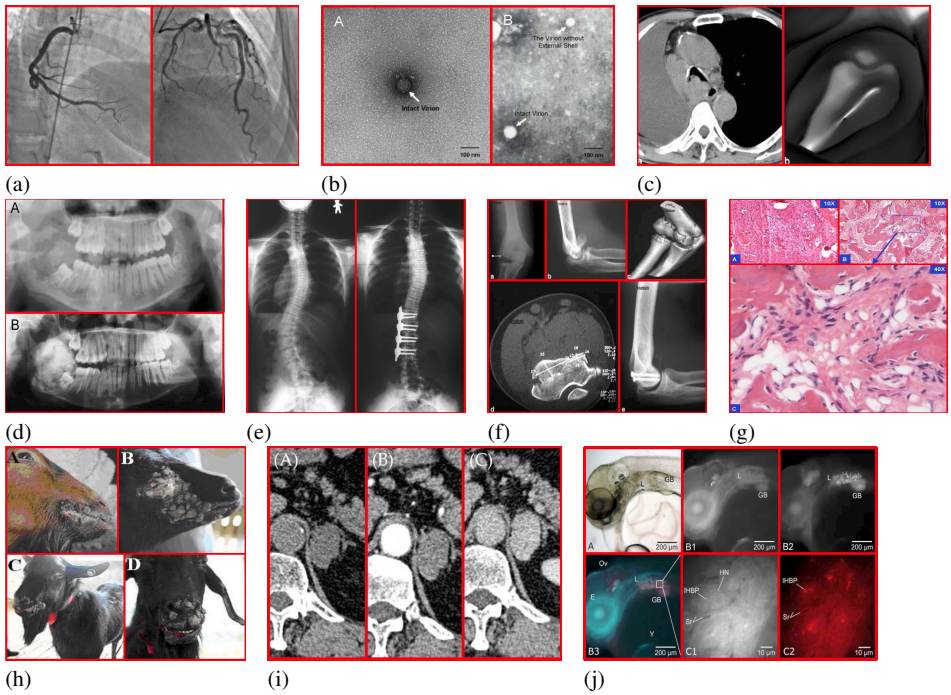

Fig. 5. Stitched multipanel figure separation, where bold lines (in red) separate subpanels. These multipanel figures corresponds to those shown in Fig 1

This means that subpanel separation is correct at least 80% OR exists. Such an OR score does not let images semantic different.

C. Results and analysis

Using the dataset of size 150 images (*cf.* Section III-A) and the evaluation protocol described in Section III-B), experimental results are reported in Table I. We have achieved precision and recall, respectively of 81.22% and 85.08% in less than 3 seconds per image, on average. All tests were made using MATLAB 2013b on Linux platform. In Fig. 5, we have shown some output examples to provide how robust the proposed system is. We remind the readers that no state-of-the-art methods reported the test on separating subpanels from these stitched multipanel figures. Consequently, no comparative study is possible.

In the reported results (see Table I), the error rate is approximately 15% (considering recall). Difficulties/challenges that cause errors can be categorized into under and over segmentation. Under segmentation occurs when no clear pixel differences exist along the subpanel boundaries (since identical backgrounds are used for all subpanels). While, over segmentation exists when clear (end to end) separation is appeared within the subpanels. In Fig. 6, both under and over segmentation problems are shown. The under segmentation problem (i.e., mainly due to identical background) can possibly be solved by intelligently integrating text panels (as implemented in refs. [16], [18]). But, this works only when OCR performs well.

TABLE I
PERFORMANCE EVALUATION (IN%).

Precision	81.22
Recall	85.08
F_1-score	83.10

IV. CONCLUSION

In this paper, we have presented a novel technique based on line segment detection and line vectorization to separate subpanels from the stitched multipanel figures. Line segments are detected locally based on the information about gray-level pixel change between the neighboring pixels, which is followed by line vectorization process that connects all broken lines along the subpanel boundaries. Considering the dataset, the proposed technique provides precision and recall of 81.22% and 85.08%, respectively, in less than 3 seconds per image, on average. Based on our experience, no state-of-the-art methods reported the use of image processing techniques to separate subpanels from these stitched multipanel figures.

Since execution time largely depends on the size of the image, we recommend to scale down the image size, prior to this technique. This allows efficient tool integration with the NLM's *Open-i* search engine, which is considered as a precursor to CBIR.

ACKNOWLEDGEMENTS

This research was supported by the Intramural Research Program of the National Institutes of Health (NIH), National Library of Medicine (NLM), and Lister Hill National Center for Biomedical Communications (LHNCBC).

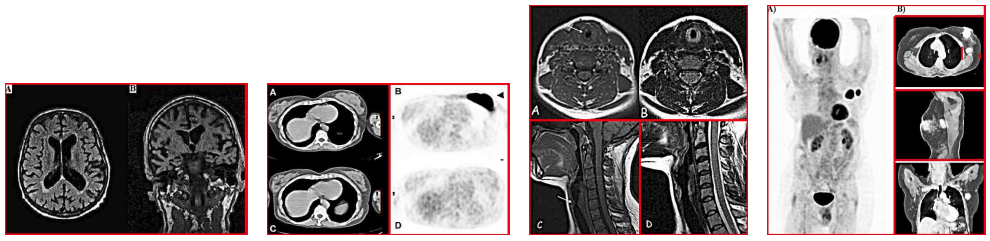

(a) (b) (c) (d)

Fig. 6. Output examples, showing (a-c) under and (d) over segmentation. Under segmentation is due to the use of an identical background for all subpanels and over segmentation is due to the existence of clear boundary between the objects within the subpanel.

REFERENCES

[1] P. Aigrain, H. Zhang, and D. Petkovic, "Content-based representation and retrieval of visual media: A state-of-the-art review," *Multimedia Tools and Applications*, vol. 3, no. 3, pp. 179–202, 1996.

[2] H. Müller, N. Michoux, D. Bandon, and A. Geissbühler, "A review of content-based image retrieval systems in medical applications - clinical benefits and future directions," *I. J. Medical Informatics*, vol. 73, no. 1, pp. 1–23, 2004.

[3] H. Müller, "Medical (visual) information retrieval," in *Information retrieval meets information visualization, winter school book*, ser. Springer LNCS, vol. 7757, 2013, pp. 155–166.

[4] A. Chhatkuli, D. Markonis, A. Foncubierta-Rodríguez, F. Meriaudeau, and H. Müller, "Separating compound figures in journal articles to allow for subfigure classification," in *SPIE, Medical Imaging*, 2013.

[5] M. S. Simpson, D. Demner-Fushman, S. Antani, and G. R. Thoma, "Multimodal biomedical image indexing and retrieval using descriptive text and global feature mapping," *Inf. Retr.*, vol. 17, no. 3, pp. 229–264, 2014.

[6] J. C. R. Licklider, "A picture is worth a thousand words: And it costs..." in *Proceedings of the Joint Computer Conference*, ser. AFIPS '69 (Spring). New York, NY, USA: ACM, 1969, pp. 617–621.

[7] J. A. Aucar, L. Fernandez, and C. Wagner-Mann, "If a picture is worth a thousand words, what is a trauma computerized tomography panel worth?" *The American Journal of Surgery*, vol. 6, no. 194, pp. 734–740, 2007.

[8] H. Yu, "Towards answering biological questions with experimental evidence: automatically identifying text that summarize image content in full-text articles," 2006, pp. 834–838.

[9] M. S. Cooper, G. Sommers-Herivel, C. T. Poage, M. B. McCarthy, B. D. Crawford, and C. Phillips, "The zebrafish {DVD} exchange project: A bioinformatics initiative," vol. 77, pp. 439 – 457, 2004.

[10] J. Kalpathy-Cramer, H. Müller, S. Bedrick, I. Eggel, A. G. S. de Herrera, and T. Tsikrika, "Overview of the CLEF 2011 medical image classification and retrieval tasks," in *CLEF 2011 Labs and Workshop, Notebook Papers, 19-22 September 2011, Amsterdam, The Netherlands*, ser. CEUR Workshop Proceedings, V. Petras, P. Forner, and P. D. Clough, Eds., vol. 1177, 2011.

[11] H. Müller, A. G. S. de Herrera, J. Kalpathy-Cramer, D. Demner-Fushman, S. Antani, and I. Eggel, "Overview of the imageclef 2012 medical image retrieval and classification tasks," in *CLEF 2012 Evaluation Labs and Workshop, Online Working Notes, Rome, Italy, September 17-20, 2012*, ser. CEUR Workshop Proceedings, P. Forner, J. Karlgren, and C. Womser-Hacker, Eds., vol. 1178, 2012.

[12] A. G. S. de Herrera, J. Kalpathy-Cramer, D. Demner-Fushman, S. Antani, and H. Müller, "Overview of the imageclef 2013 medical tasks," in *Working Notes for CLEF 2013 Conference , Valencia, Spain, September 23-26, 2013.*, ser. CEUR Workshop Proceedings, P. Forner, R. Navigli, D. Tufis, and N. Ferro, Eds., vol. 1179. CEUR-WS.org, 2013.

[13] C. B. Akgül, D. L. Rubin, S. Napel, C. F. Beaulieu, H. Greenspan, and B. Acar, "Content-based image retrieval in radiology: Current status and future directions," *J. Digital Imaging*, vol. 24, no. 2, pp. 208–222, 2011.

[14] D. Demner-Fushman, S. Antani, M. S. Simpson, and G. R. Thoma, "Design and development of a multimodal biomedical information retrieval system," *Journal of Computing Science and Engineering*, vol. 6, no. 2, pp. 168–177, 2012.

[15] M. M. Rahman, D. You, M. S. Simpson, S. Antani, D. Demner-Fushman, and G. R. Thoma, "Interactive cross and multimodal biomedical image retrieval based on automatic region-of-interest (ROI) identification and classification," *Int. J. Multimed. Info. Retr.*, vol. 3, no. 3, pp. 131–146, 2014.

[16] L. D. Lopez, J. Yu, C. N. Arighi, C. O. Tudor, M. Torii, H. Huang, K. Vijay-Shanker, and C. H. Wu, "A framework for biomedical figure segmentation towards image-based document retrieval," *BMC Systems Biology*, vol. 7, no. S-4, p. S8, 2013.

[17] B. Cheng, S. Antani, R. J. Stanley, and G. R. Thoma, "Automatic segmentation of subfigure image panels for multimodal biomedical document retrieval," in *Document Recognition and Retrieval XVIII - DRR 2011, 18th Document Recognition and Retrieval Conference, part of the IS&T-SPIE Electronic Imaging Symposium, San Jose, CA, USA, January 24-29, 2011, Proceedings*, ser. SPIE Proceedings, G. Agam and C. Viard-Gaudin, Eds., vol. 7874, 2011, pp. 1–10.

[18] E. Apostolova, D. You, Z. Xue, S. Antani, D. Demner-Fushman, and G. R. Thoma, "Image retrieval from scientific publications: Text and image content processing to separate multipanel figures," *JASIST*, vol. 64, no. 5, pp. 893–908, 2013.

[19] R. F. Murphy, M. Velliste, J. Yao, and G. Porreca, "Searching online journals for fluorescence microscope images depicting protein subcellular location patterns," in *Proceedings of the 2nd IEEE International Symposium on Bioinformatics and Bioengineering*, ser. BIBE '01, 2001, pp. 119–128.

[20] R. Grompone von Gioi, J. Jakubowicz, J.-M. Morel, and G. Randall, "LSD: a Line Segment Detector," *Image Processing On Line*, vol. 2, pp. 35–55, 2012.

[21] C. Hendriks and L. Vliet, "Discrete morphology with line structuring elements," in *Int. Conf. on Computer Anal. of Images and Patterns*, ser. Lecture Notes in Computer Science, N. Petkov and M. Westenberg, Eds. Springer Berlin Heidelberg, 2003, vol. 2756, pp. 722–729.

[22] C. Harris and M. Stephens, "A combined corner and edge detector," in *4th Alvey Vision Conference*, 1988, pp. 147–151.

[23] L. R. Dice, "Measures of the amount of ecologic association between species," *Ecology*, vol. 26, no. 3, pp. pp. 297–302, 1945.